Experimental Reexamination of Transverse Tensile Strength for IM7/8552 Tape-Laminate Composites

Caitlin M. Arndt[1], Nelson V. De Carvalho[2], Michael W. Czabaj[1*]

[1]Department of Mechanical Engineering, University of Utah, Salt Lake City, UT 84112.
[2]National Institute of Aerospace, Hampton, VA 23681.
*Corresponding Author: m.czabaj@utah.edu

ABSTRACT

Due to the observed dependence of transverse-tensile strength, Y_T, on test geometry and specimen size, there is no consensus regarding a test method that can uniquely measure Y_T. This study reexamines characterization of Y_T by comparing results from established flexure tests with results from a new tensile test that exhibits consistent failure in the gage region. Additionally, the effects of surface preparation and direction of transverse fracture are investigated. Results show that Y_T is inversely proportional to specimen volume and surface roughness, and is insensitive to direction of transverse fracture. The relationship between specimen volume and Y_T is adequately captured by Weibull strength-scaling theory, except at the tails of the Y_T distributions. However, specimens exhibited microcracking prior to failure, which violates the "weak-link" assumptions of the Weibull theory. These findings highlight the challenges of using deterministic Y_T values in progressive damage analysis.

1. INTRODUCTION

Transverse tensile fracture is one of the most frequently observed failure modes in tape-laminate polymer-matrix composites (PMCs). The propensity for this failure mode in PMCs is due to low tensile strength of the polymer matrix relative to tensile strength of the reinforcing fibers. In itself, transverse tensile fracture can lead to some degradation of laminate in-plane elastic properties, which is rarely critical. However, this failure mode can also act as a precursor to other, more severe, forms of damage including delamination, fiber tensile failure, and/or

compressive fiber kinking. As a result, characterization and accurate prediction of transverse tensile fracture is of great importance to ensure safe and reliable deployment of PMCs in primary structural applications.

One of the most common ways of predicting transverse tensile fracture is based on experimental characterization of transverse tensile strength, Y_T. In rudimentary laminate analyses (vis. first-ply failure or ply-discount models) Y_T is used directly to determine ply failure for a given state of transverse tensile stress. In more advanced, finite element (FE)-based Progressive Damage Analysis (PDA), Y_T is used to determine when individual elements begin to fail. For example, in continuum damage mechanics models, Y_T can be used in conjunction with a preferred composites failure theory (e.g. LaRC04 [1]) to determine when an element has reached a critical stress level that initiates gradual degradation of its stiffness [2]. In numerical approaches which model cracks discretely, Y_T has been used to determine the onset of the release process of pre-defined [3,4], or automatically inserted, zero-thickness cohesive elements [5-8] or zones [9]. Both continuum and discrete approaches typically use a combination of Y_T, along with mode-I fracture toughness, G_{Ic}, to define a traction-separation law that governs onset and subsequent material degradation [10-11]. The simulation of crack propagation using traction-separation laws leads to the development of a process zone, within which the material has initiated its degradation, but traction-free crack faces have not yet formed. Variations in the process zone length have been demonstrated to affect the solution, particularly in the first stages of growth as the process zone is formed [12]. For the same assumed G_{Ic} and traction law shape, a higher/lower Y_T results in a smaller/larger process zone. Hence, the choice of Y_T can affect the solution beyond the onset and into the initial stages of crack growth. Furthermore, from a practical perspective, the adequate representation of the process zone imposes restrictions on the

maximum element size that can be used [13], with smaller process zones (higher Y_T) requiring finer discretizations. With a few exceptions (e.g. [14]), nearly all analysis approaches assume a single deterministic value for Y_T. Despite widespread use of Y_T for prediction of intra-laminar fracture in tape-laminate PMCs mentioned above, a number of studies have demonstrated that obtaining this parameter is not straightforward.

Currently there is no consensus in the literature regarding which test method should be used to measure Y_T, and how to deal with dependence of this property on the specimen size and geometry. To date, the most widely accepted method for characterization of Y_T, described in the ASTM standard D3039, involves uniaxial loading of unidirectional transverse specimens [15]. According to D3039, test specimens require a constant rectangular cross-section, which must be gripped using tabs to prevent splitting at the points of load introduction. Although this test is relatively easy to perform, several studies have observed that specimens often fail near or at the loading tabs, and that size of specimen cross-section has an effect on the magnitude of the measured Y_T [16-18]. For example, in a study by O'Brien and Salpekar, a series of carbon/epoxy specimens with varying widths and thicknesses were tested according to ASTM D3039. In this study, nearly 22% of tested specimens broke at or near the loading tabs, and the coefficient of variation for Y_T was as large as 19%. Despite the scatter in the data, Y_T appeared to decrease with the increasing gage region thickness, but changes in width did not have an effect on Y_T [16].

The second most common way of measuring Y_T involves flexure loading of unidirectional transverse beams. Relative to ASTM D3039, fabrication and testing of flexure specimens is simpler since no additional tabbing is required, provided that large enough loading rollers are used. Typically, flexure testing is performed using 3-point bend (3PB) or 4-point bend (4PB) fixture configurations, and data reduction is based on the beam theory. A study by O'Brien et al.

examined the difference between 3PB and 4PB configurations using glass/epoxy and carbon/epoxy specimens [19]. For both material systems and test types, Y_T decreased with increasing specimen width, thickness, and support span; however, the observed trends were somewhat obscured by the specimen-to-specimen and batch-to-batch (i.e. panel-to-panel) variability. Despite the observed scatter, Y_T values obtained from 4PB tests were lower than those obtained from 3PB tests by as much as 15%. The difference between Y_T obtained from tensile and flexure testing has been investigated by Adams et al. using carbon/epoxy specimens [20]. This study observed that Y_T measured using 3PB tests was nearly twice the value obtained from tensile testing. The large difference between strengths derived from flexural and tensile tests has been observed for other PMCs systems [21-23], as well as other brittle materials like cement [24], rock [25], and ceramics [26].

The observed trend of Y_T changing with specimen size or loading type (e.g. tension versus flexure) has been related to the volume of the material subjected to tensile stresses prior to failure. This trend, known as the "size effect", is a well-documented phenomenon observed in brittle and quasi-brittle materials [27-31]. For PMCs, the size effect has been described in two comprehensive review articles by Bažant and Wisnom [32,33]. With existence of the size effect, the most common approach for relating (i.e. scaling) Y_T between different specimen volumes is the Weibull scaling law, which is based on the so-called "weakest link" theory [34,35]. The weakest link theory analogizes a brittle material to a chain composed of links in series, in which the entire chain is only as strong as its weakest link. The underlying assumption of this theory is that the strength of individual links is governed by presence of critical flaws and inhomogeneities, and thus increasing the number of links (i.e. volume of the material) increases the probability of failure.

The discussion in the literature on the applicability of the Weibull scaling law to PMCs is somewhat conflicting [36,33]. In some cases, the Weibull law provides a reasonable scaling between strengths [21,37,38], while in other cases the Weibull law fails to account for the volumetric effects. In a study by O'Brien and Salpekar [16] the Weibull scaling law was applied to compare Y_T values to those previously obtained by Crews [39] using a flexure test on 90° specimens. It was found that the analytical solution for the effective stressed volume did a poor job of scaling the characteristic Y_T, but approximating a larger effective volume of the entire width, length, and half of the beam depth gave reasonable strength predictions. While this approach may have given better results than using the calculated effective volume, it is not consistent with the statistical theory. In another study, O'Brien et al. applied Weibull theory to scale strength between 3PB and 4PB specimens [19]. They found that the Weibull scaling law over-predicted the change in Y_T, both when scaling between similar testing configurations (e.g. 3PB tests with varying spans), and when scaling between different test configurations (e.g. 3PB versus 4PB). They concluded that Weibull scaling did not adequately capture the size effects for PMCs.

The above discussion raises several interesting considerations related to experimental characterization and the use of Y_T. First, based on current literature, it is unclear which test should be used to measure Y_T. For instance, tensile testing using D3039 results in low, and thus conservative, values of Y_T; however, the frequent failure near the loading tabs casts doubt on the validity and repeatability of this test. Conversely, existing flexure tests appear to be very repeatable, yet they produce unusually high values of Y_T, which must be scaled down to represent behavior of the bulk material. Second, the difficulty of measuring Y_T has resulted in a lack of consensus on whether the existing volumetric scaling laws (e.g. Weibull) can be used to

effectively scale Y_T. Without this consensus, it is currently unclear how to best use Y_T in existing failure prediction models.

In view of these considerations, the main goal of this study is to reexamine experimental characterization of Y_T for tape-laminated composites. Consequently, the presented work has two main objectives: (1) re-characterization of Y_T for a common carbon/epoxy (viz. IM7/8552) system using both flexure and tensile tests, and (2) observation of microscale fracture that leads to ultimate transverse tensile failure in Y_T tests. Re-characterization of Y_T is performed using specimens with different effective volumes to enable investigation of the volumetric scaling effects. Flexure testing is performed using existing 3PB and 4PB tests adopted from [19]. Tensile testing is performed using a new non-prismatic specimen adopted from [40], modified to ensure consistent failure in the gage region. In addition, the 3PB specimens are also used to examine the effect of specimen surface preparation (i.e. extent of surface flaws in unpolished vs. polished samples), and specimen orientation (i.e. out-of-plane versus in-plane transverse failure) on Y_T. The microscopic observations of fracture are performed by conducing *in-situ* and *ex-situ* imaging of the flexure specimens using optical microscopy. These observations are performed with aim of discovering the microscale failure mechanisms (e.g. microcracking) that contribute to macroscopic transverse tensile failure of specimens, and which may provide insight into validity of the existing scaling laws.

In what follows, Section 2 presents the test methods, details regarding specimen fabrication and preparation, and a summary of the tests performed. Section 3 provides an overview of two-parameter Weibull scaling and its application to the geometries tested. Section 4 presents and discusses the experimental results, and is followed by concluding remarks in Section 5.

2. METHODS

The characterization of Y_T was performed using 3PB, 4PB, and tensile test configurations. The data obtained from all three tests are used to investigate the relationship between the effective volume (i.e. volume subjected to tensile stresses) and Y_T. Similarly, data from these tests are used to assess the suitability of the two-parameter Weibull theory to model and scale the stochastic distribution of Y_T. In addition, 3PB and 4PB tests were used to investigate the microscale fracture processes occurring before reaching the critical failure load used to calculate Y_T. Finally, 3PB tests were used to investigate the effects of surface preparation and specimen orientation on Y_T.

2.1 Specimen fabrication and surface preparation

The material system used in this study was Hexcel's IM7/8552 unidirectional prepreg with 35% resin content and 190 gsm areal weight. This material was selected for this study due to its widespread presence in the composites research literature. Given the large number of samples required for this study, three unidirectional laminates were fabricated and machined into test specimens. The three 305×305 mm unidirectional laminates, two 20-ply and one 26-ply, were cured according to NCAMP's specification [41]. The laminates were cured in an autoclave at temperature of 177 °C, 586 kPa part pressure, and 137.9 kPa vacuum. All cures were performed in a PTFE-coated steel mold which resulted in a smooth finish on the laminate surfaces. The resulting nominal plate thicknesses were 3.59 mm and 4.73 mm for the 20- and 26-ply laminates, respectively. The fiber volume fraction for each laminate was determined visually based on optical microscopy. The resulting fiber-volume fractions were 55.6% and 56.0% for the 20- and 26-ply laminates respectively.

After cure, all 20-ply laminate specimens were water-jetted, while all 26-ply specimens were cut using a 1.3-mm-thick diamond blade. After initial machining, all flexural and tensile specimens were lightly sanded using 800-grit silicon carbide sandpaper to remove surface scratches and fiber-blowout from machining. As detailed in the next section, a portion of flexure specimens were subsequently sanded using a 1200-grit silicon carbide sandpaper, and polished using a lapping cloth coated with a mixture of 0.05 micron alumina powder, water, and dish soap. After polishing, all samples were examined using a Keyence VHX-5000 optical microscope. An example view of the polished 2-3 (out-of-plane) and 1-2 (in-plane) surfaces imaged at ~0.1μm/pixel resolution are shown in Fig. 1.

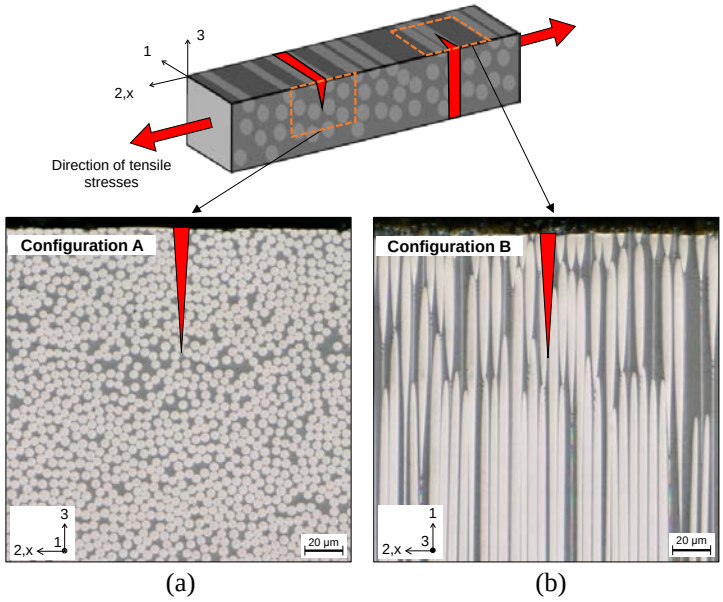

Figure 1. Example of final polish surfaces on (a) the 2-3 and (b) 1-2 planes imaged with Keyence VHX-5000 optical microscope. Red regions indicate direction of transverse fracture in configuration A and B specimens.

2.1.1 Flexure tests

The specimen geometry and the experimental setup for the 3PB and 4PB tests are shown in Fig. 2. As shown this figure, the outer span for both tests was 25.4 mm, the inner span for the 4PB test was 8.5 mm, and all rollers were 4 mm in diameter. All specimens were nominally 31.8 mm long. Prior to sanding and polishing, the width of all specimens was nominally 5.0-5.5 mm,

while the specimen thickness was nominally 3.59 and 4.73 mm for the 20- and 26-ply plate specimens, respectively. The majority of flexure specimens were tested in configuration "A", where specimen fiber direction was aligned with the specimen's width (see Figs. 1a and 2). A selected few specimens were tested in configuration "B" where specimen fiber direction was aligned with the specimen's thickness (see Figs. 1b and 2). This was done to investigate whether transverse failure is influenced by the direction of expected fracture path (i.e. 3-direction for configuration A versus 1-direction for configuration B).

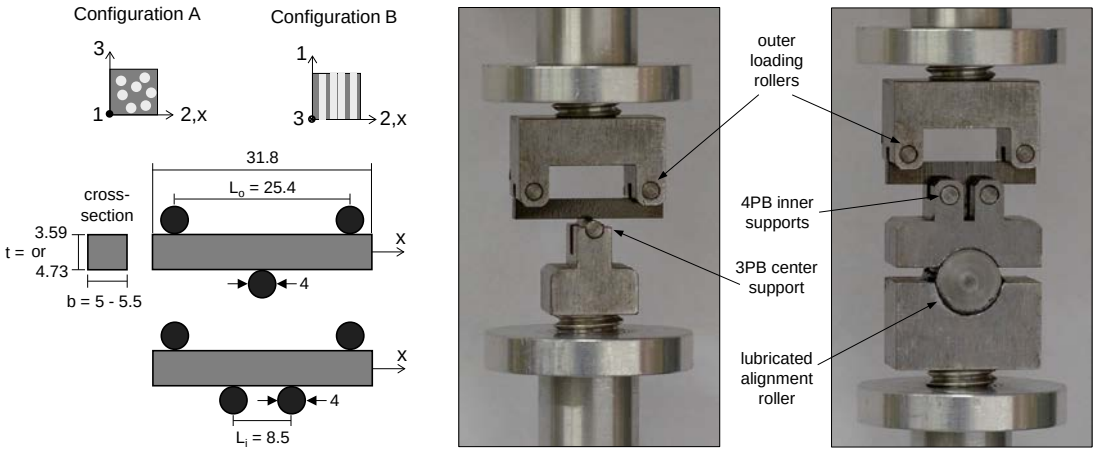

Figure 2. Nominal specimen geometry and the experimental setup for the 3PB and 4PB tests (all units in mm).

All flexure tests were performed in an Instron ElectroPuls E1000 load-frame equipped with a 1 kN load cell. As shown in Fig. 2, both tests were inverted to ensure that the center (loading) rollers remained stationary. This configuration, based on location of the actuator in the E1000, restricted the vertical displacement of samples in the central tensile region, and enabled *in-situ* imaging. All flexure specimens from the 26-ply laminate were polished to a mirror-finish and imaged *in-situ* in the area of the expected tensile failure using a custom traveling microscope equipped with a 10X objective lens and PointGrey Grasshopper GRAS-50S5M-C 5-megapixel camera. The lens-camera configuration allowed for a field-of-view of approximately 0.88 mm ×

0.75 mm, which made individual fiber cross-sections easily distinguishable (~0.36 μm/pixel resolution). All specimens were loaded in displacement control at a rate of 0.15 mm/min.

Two different methods were used to acquire images during *in-situ* flexure testing of the 26-ply polished specimens. The first method involved acquiring and overlapping images across the specimen tensile side, approximately 9 images in either direction. Following testing, these images were stitched together to create a 10.75 mm × 0.75 mm mosaic that provided high-resolution macroscale view of the specimen. Because of the labor-intensive nature of this process, only a few samples were imaged this way. The second method involved acquiring a single image in the center of each specimen on the tensile side. For both methods, reference images were taken at 13 N, and subsequent microscale imaging started at 133 N, and repeated every 44.5 N until failure. Following *in-situ* imaging, for each sample, the microscale images obtained at different loads were combined into an image stack in an image-processing program ImageJ [42], and aligned using a template-matching algorithm [43]. Alignment of images enabled visual detection of pre-existing and newly formed microscale cracks.

In addition to making *in-situ* surface observations mentioned above, a special 3PB fixture was developed to investigate formation of internal microscale cracking across the specimen's width. This fixture, shown in Fig. 3, was designed to hold the specimen flexed at approximately 80% of average failure load using aluminum picture-frame and a quick-curing Buehler's SamplKwick two-part acrylic resin. After curing the acrylic resin at load, the specimen and the picture-frame were subsequently removed from the load-frame, and serial-sectioned in the width direction using 0.1 mm increments. The imaging was done on the tensile side using Keyence VHX-5000 optical microscope at ~0.1μm/pixel resolution.

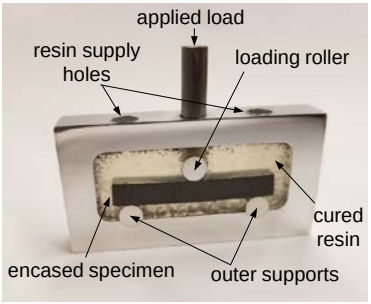

Figure 3. Test setup used to investigate formation of internal microscale cracking across specimen's width

2.1.2 Tensile tests

The specimen geometry and the experimental setup for the tensile tests are shown in Fig. 4. As shown this figure, the tensile specimens were nominally 53 mm long and 16 mm wide at the widest. The central gage region was 35 mm long and contained a 97 mm constant-radius fillet on both sides. This resulted in a 2.0 mm nominal width at the narrowest point. The filleted gage region ensured localized failure in the center of the gage region and away from the grip interfaces. The nominal specimen thickness prior to polishing was 3.59mm. The specimens were loaded using open-face steel grips with 45° tapered faces which ensured specimen alignment [40]. All tensile tests were performed in displacement control at a rate of 0.15 mm/mm using Instron ElectroPuls E1000 load-frame equipped with a 1 kN load cell.

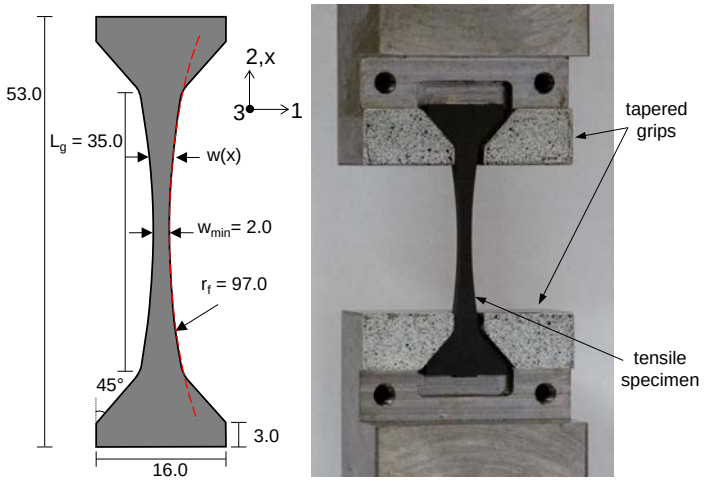

Figure 4. Specimen geometry and the experimental setup for the tensile tests (all units in mm)

2.2 Test matrix

A summary of the entire test matrix is presented in Table 1. In this table, the plate name indicates the number of plies used in each laminate. For the 20-ply geometry, two laminates were fabricated and these are additionally indicated with "-1" or "-2". The 20- and 26-ply laminates are treated as separate due to different lots (i.e. rolls) of prepreg used to manufacture each plate type. Finally, all polished samples are marked with a "*", while specimens used to examine the difference in the out-of-plane or the in-plane Y_T are indicated with superscripts "A" and "B", respectively.

Table 1. The test matrix

	3PB		4PB		Tension
Study/plate name	**20-1/-2**	**26**	**20-1/-2**	**26**	**20-1/-2**
Volumetric effects and Weibull scaling	36	–	37	–	39
Micromechanical observations	–	25^{*}	–	25^{*}	–
Effect of surface preparation	6^{*}, 36	–	–	–	–
Effect of specimen orientation	–	36^{*}, 10^{B*}	–	–	–

*indicates polished. All flexure specimens are configuration A unless otherwise noted.

3. TWO-PARAMETER WEIBULL SCALING MODELS

In this study, the experimentally measured Y_T data was used to assess the suitability of Weibull statistical strength theory [34] to predict the apparent strength of different specimen geometries. Other cumulative functions have been proposed in the literature and applied to strength scaling in composites, e.g. [44]. In the present work, the two parameter cumulative function was selected due to its widespread use in the composites community and relative simplicity. In view of the fact that this theory has been described extensivly in the open literature [36,45-47], only a few key equations are presented here for brevity.

Following [34], the probablity of failure P as a function of applied stress σ is assumed to be described by a general two-parameter Weibull cumulative distribution function

$$P(\sigma) = 1 - e^{\left[-\int_V \left(\frac{\sigma}{\sigma_0}\right)^m dV\right]}, \tag{1}$$

where V is the specimen's volume, σ_0 is the scale parameter and m is the shape parameter or "Weibull modulus" which describes dispersion of the strength data. For a given specimen, Eq. 1 is typically written as

$$P(\sigma) = 1 - e^{\left[-\left(\frac{\sigma}{\sigma_c}\right)^m\right]}, \tag{2}$$

where σ_c, the characteristic strength of the specimen, and m can be estimated based on least-squares regression or maximum likelihood estimation [48]. It follows from Eq. 1 that the characteristic strength of two specimens under uniform loading, made from the same material, but with different volumes, V_1 and V_2, can be related according to the following scaling law

$$\sigma_{c,1} = \sigma_{c,2}\left(\frac{V_2}{V_1}\right)^{\frac{1}{m}}. \tag{3}$$

For specimens loaded with a non-uniform stress field, Eq. 1 can be used to determine an effective volume that, if loaded with a uniform stress field, would result in the same scaling in characteristic strength as obtained in the specimen loaded with a non-uniform stress field. Assuming that only tensile loads can cause failure, the effective volumes of the 3PB and 4PB configurations are given by

$$V_{eff-3PB} = V_{3PB}\frac{1}{2(m+1)^2}, \tag{4}$$

$$V_{eff-4PB} = V_{4PB}\frac{\frac{L_i}{L_0}m+1}{2(m+1)^2}, \tag{5}$$

where L_i is the distance between the two inner rollers in the 4PB test, L_0 is the distance between the outer rollers, and V_{3PB} and V_{4PB} are the specimen volumes between outer rollers for the 3PB and 4PB specimens, respectively. The reader is directed to references [45,46] for a detailed derivation of these expressions.

A procedure similar to the one used to derive Eqs. (4) and (5) was followed to obtain an expression for the effective volume of the tensile specimen, $V_{eff\text{-}T}$. To simplify this calculation, the effective volume was assumed to be within the gage region L_g = 35 mm, as shown in Fig. 4. Within this region, the specimen width, $w(x)$, follows a power-law expression

$$w(x) = w_{\min}(\alpha x^2 + 1), \tag{6}$$

where $\alpha = 1/(2r_f w_{min})$, r_f is the radius of the fillet, and w_{min} is the minimum specimen width, as shown in Fig. 4. In addition, based on elastic FE analysis of the tensile specimen geometry, it was assumed that the tensile stress was constant across the specimen's width and depth at any point along the gage region. With these assumptions, the expression for stress in the gage region is given by

$$\sigma(x) = \frac{N}{tw(x)} = \frac{\sigma_{\max}}{\alpha x^2 + 1}, \tag{7}$$

where N is the applied load, t is the specimen thickness, and $\sigma_{max} = N/(tw_{min})$ is the maximum stress within the gauge region. Equation 7 was substituted into Eq. 1, and subsequently integrated to obtain the effective volume for the tensile specimen

$$V_{eff-T} = tw_{\min} L_g \; {}_2F_1\left(\frac{1}{2}, m-1; \frac{3}{2}; -\left(\frac{L}{2}\right)^2 \alpha\right), \tag{8}$$

where ${}_2F_1$ is the hypergeometric function [49]. The equations for effective volumes $V_{eff\text{-}3PB}$, $V_{eff\text{-}4PB}$, and $V_{eff\text{-}T}$ can be used directly in Eq. 3 to scale between the characteristic strengths of the three specimen geometries considered.

4. RESULTS AND DISCUSSION

4.1 Transverse tensile strength

For the 3PB and 4PB tests, Y_T was calculated using the following beam theory expressions

$$Y_T^{3PB} = \frac{3N_{cr}L_0}{2bt^2}, \tag{9}$$

$$Y_T^{4PB} = \frac{N_{cr}L_0}{bt^2}, \tag{10}$$

where N_{cr} is the critical force at the onset of macroscopic specimen failure, b is the specimen width, and t is the specimen thickness. A discussion on the applicability of these equations for calculation of Y_T can be found in the work by O'Brien and Krueger [50]. For the tensile test, Y_T was calculated in the narrowest part of the specimen using

$$Y_T^{tensile} = \frac{N_{cr}}{w_{\min}t}. \tag{11}$$

Figure 5 shows stress-displacement curves obtained from flexure and tensile testing of all unpolished 20-ply specimens. As seen in this figure, the macroscopic failure was defined by a large drop in the stress. In all specimens, including those from tensile tests, failure always occurred in the gage region (i.e. region of magnified tensile stress). For the 3PB specimens, failure sites were within 0.7±0.6 mm from the central roller. For 4PB specimens, failure sites were uniformly distributed between the two inner rollers, with a few specimens breaking within 0.8 mm outside the inner rollers. The location of failure sites for both flexure specimens was similar to that observed in Ref. [19]. For tensile tests, average failure site was within ± 2.3 mm

from the narrowest part of the gage region. Detailed *in-situ* microscopic observations showed some amount of microcracking prior to catastrophic failure in nearly all specimens observed (see Section 4.3); however, no measurable change in specimen compliance was detected. The initial nonlinearity observed during tensile tests (Fig. 5c) was related to specimen settling within the tapered grips.

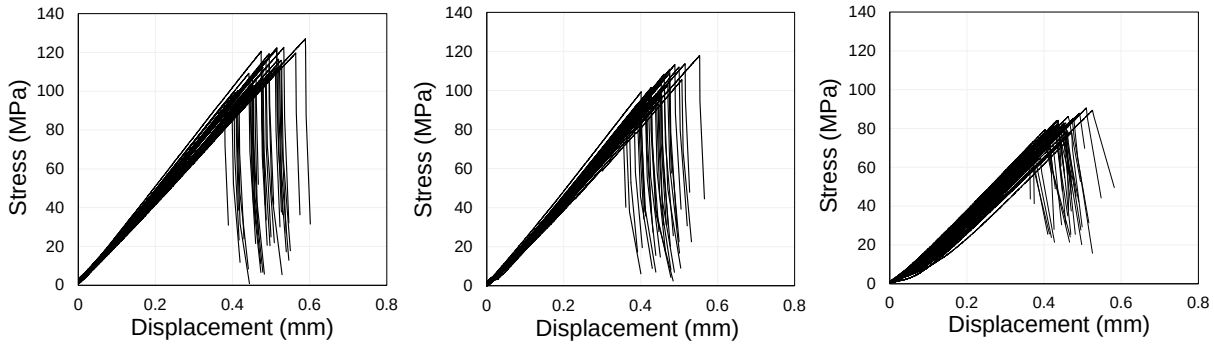

(a) 3PB flexure (b) 4PB flexure (c) tension

Figure 5. Force-displacement data from flexure and tensile testing of 20-ply unpolished specimens.

Table 2 and Fig. 6 summarize the transverse tensile strength test results. In Table 2, columns 1-5 present the type and number of tests performed, as well as the as-measured average dimensions of the unpolished specimens. Columns 6 and 7 present the mean and scatter of Y_T calculated based on Eqs. 9-11. Columns 8 and 9 give σ_c and m obtained by performing a 2-parameter-Weibull fit to the measured Y_T values using Matlab's '*wblfit*' function [51]. Finally, column 10 presents the average effective volume for each configuration calculated based on Eqs. 4, 5 and 8. Figure 6a shows the characteristic strength, σ_c, with the error bars corresponding to the maximum and minimum values of Y_T; while Fig. 6b shows the Y_T data on a Weibull plot. In Fig. 6b each symbol corresponds to a Y_T value obtained from an individual specimen, while the straight lines indicate the Weibull fit with the Weibull modulus, m, as shown on the bottom of each curve.

Table 2. Summary of transverse tensile strength from 3PB, 4PB, and tensile tests.

Test type	Number tested	b^{ave} (mm)	t^{ave} (mm)	$w_{min}{}^{ave}$ (mm)	$Y_T{}^{ave}$ (MPa)	CV (%)	σ_c (MPa)	m	$V_{eff}{}^{ave}$ (mm^3)
3PB	36	5.19	3.24	-	108.3	8.6	112.6	12.80	1.12
4PB	37	5.20	3.41	-	98.8	9.4	102.9	11.89	6.40
tensile	39	-	2.99	2.10	78.7	8.5	81.5	14.68	62.45

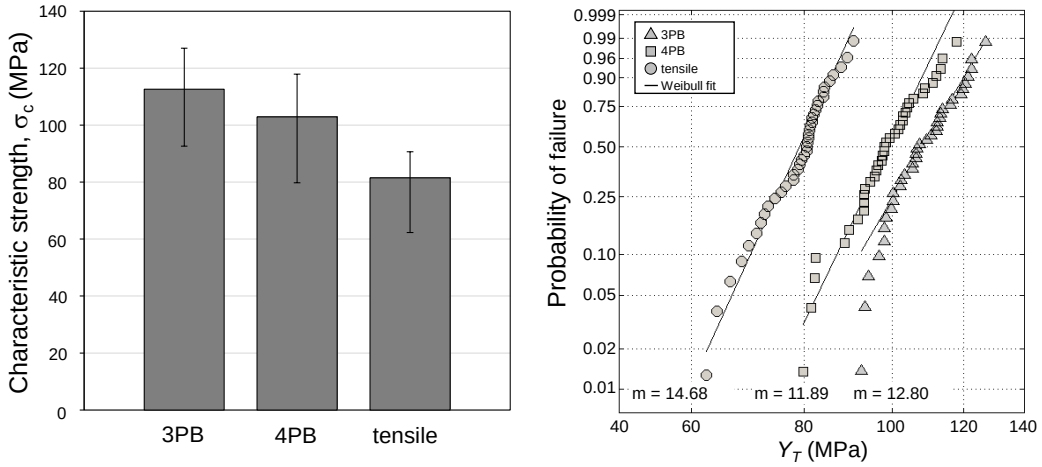

(a) (b)

Figure 6. Transverse tensile strength test results showing (a) characteristic strength σ_c with error bars corresponding to maximum and minimum values of Y_T, and (b) best fit of a 2-parameter-Weibull cumulative distribution function.

Examining Table 2, the average values and scatter of Y_T are within the bounds of what was previously reported for this material system [19,52]. Examining Table 2, there is a very clear trend of decreasing Y_T with increasing effective specimen volume, especially between flexure and tensile tests. In Fig. 6b, the effect of increasing volume is indicated by the leftward shift of the individual data sets. Examining Fig. 6b, the two-parameter Weibull model does a relatively good job of predicting intermediate values of Y_T, but it provides a rather poor fit at the tails of each distribution. Additionally, the Weibull slopes are different for each test geometry, which seems to contradict the notion that this parameter is a material constant. Overall, the Weibull slopes obtained from the flexure tests were slightly less than those reported in [19] for the same material type. Note that the poor fit of the low strength values presented in Fig. 6b (i.e. left tail end) can be improved by using a three-parameter Weibull model [53], however, additional testing would be required to improve estimation of the location parameter.

After initial data analysis, Equation 3 was used to scale the characteristic strength values between the three different specimen configurations. In other words, for each test geometry, the corresponding characteristic strength (i.e. σ_c^{test}) and Weibull modulus (i.e. m^{test}) were used to predict the characteristic strength for the remaining two test geometries. The results of this scaling are summarized in Table 3 and Fig. 7.

Table 3. Weibull scaling of the characteristic strength between the three test geometries

Test type	Measured σ_c (MPa)	σ_c predicted from 3PB (MPa)	% error	σ_c predicted from 4PB (MPa)	% error	σ_c predicted from tensile (MPa)	% error
3PB	112.6	–	–	119.1	5.8	107.2	-4.8
4PB	102.9	98.3	-4.5	–	–	95.2	-7.5
tensile	81.5	82.2	0.9	85.0	4.3	–	–

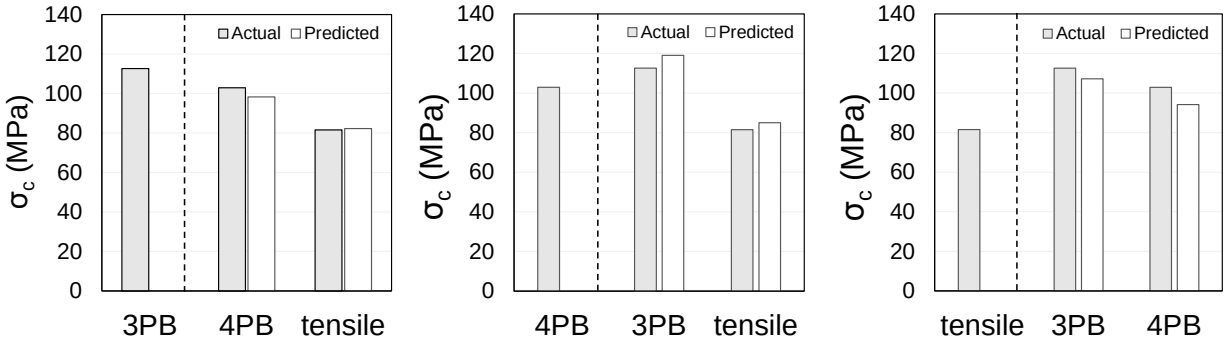

Figure 7. Weibull scaling of the characteristic strength between the three test geometries

In general, when scaling between the two flexure configurations, the percentage difference is relatively low and around 5%. The scaling under-predicts σ_c^{4PB} based on the 3PB configuration, and over-predicts σ_c^{3PB} based on the 4PB configuration, which is the same relationship observed by O'Brien et al. [19]. In general, the flexure tests data over-predict $\sigma_c^{tensile}$ by 0.9-4.3%, while the tensile test data under-predicts the flexure test data by 4.8-7.5%. Based on these results, one can conclude that the two-parameter Weibull law does a relatively good job of scaling the characteristic strength between the three geometries tested in this study. However, as mentioned before, this model does a poor job of predicting, and therefore scaling, tail ends of Y_T

distributions, which may result in relatively conservative predictions of transverse failure initiation.

4.2 Effect of polishing and specimen orientation

The effects of surface preparation and specimen orientation on Y_T are summarized in Figure 8. As seen in Fig. 8a, Y_T increases by approximately 36.5% when the specimens are polished to a mirror finish. Although a limited number of 3PB specimens were used to reach this conclusion (see Table 1), a *p*-value hypothesis test indicated this difference is statistically significant. Assuming that polishing affects Y_T, an interesting consideration arises regarding which surface preparation is more representative of a typical laminate. One can speculate that the type and frequency of flaws in the subsurface plies is much different relative to the surface plies; and therefore, selection of Y_T (i.e. either from unpolished or polished specimens) in PDA must be done judiciously depending on the expected damage location.

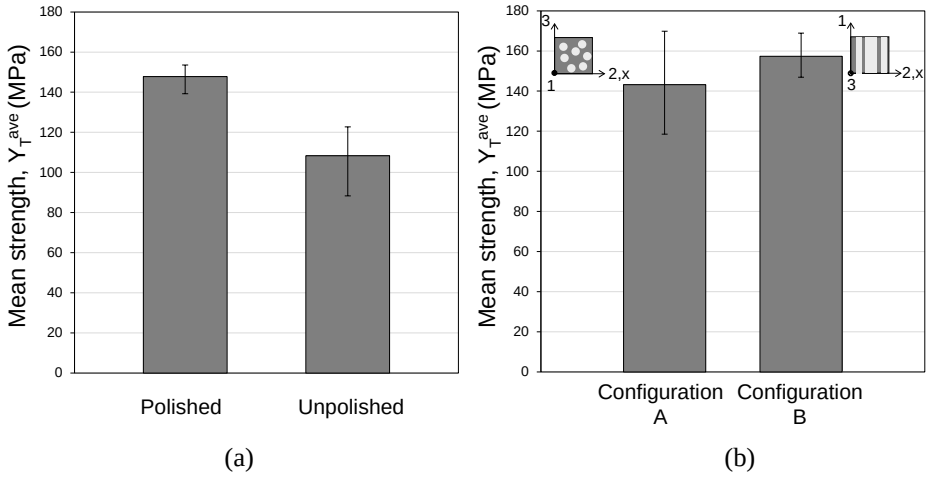

Figure 8. Effects of surface preparation and specimen orientation on Y_T^{ave}. Error bars correspond to maximum and minimum values of Y_T.

Examining Fig. 8b, there appears to be little difference between Y_T obtained from configuration A and B specimens. As seen in this figure, configuration B specimens appear to be slightly stronger on average; however, this difference can be partly attributed to a 6.5% larger volume of the configuration A specimens. The similarity between the two configuration types is

not unexpected, and has been observed previously for other matrix-dominated properties in IM7/8552 [54].

The values shown in Fig. 8 provide insight into the effects of specimen polishing and orientation on Y_T; nevertheless, a larger set of tests would be valuable to strengthen further the statistical significance of these findings. In particular, a larger data set may provide additional information on the tail ends of Y_T distributions, however this was beyond the scope of this work.

4.3 Microscale observations

All microscale *in-situ* observations were performed using flexure specimens in the A-configuration (i.e. fibers aligned with the specimen width). Tensile specimens were not imaged due to difficulty in polishing the filleted 2-3 surface prior to testing. During testing, a majority of flexure specimens were imaged using a "single-image" method, while a selected few specimens were imaged over a larger area using the "multi-image" approach (see Sec. 2.1.1). The single-image observations, performed over a central 0.88 mm × 0.75 mm region, revealed that nearly 65% of all specimens exhibited microscale cracking prior to reaching the critical load used to calculate Y_T. In general, 21% of these microcracks were pre-existing, 79% formed during loading, and all cracks had to be at least 5-10 μm long to be observed and thus recorded with high confidence. The spatial extent and evolution of the observed microcracking is illustrated in Figure 9 using images collected using the multi-image method applied to a 3PB specimen. The four images in Figure 9, each collected at a different load level, show the evolution of microcracks (symbols) overlaid on top of the underlying microstructure (background grayscale images). The height of each image is approximately 4-plies or 0.75 mm, and the width is approximately 10 mm. Each image is centered at the loading roller, as indicated by the solid white lines. The location of ultimate specimen failure was ~0.5 mm left from the center, as is

indicated by a solid red line in the bottom-most image. This specimen was imaged at seven loading intervals, but only four are shown here for brevity. At 178 N (45% of N_{cr}), 18 microcracks, marked with red squares, were observed within the imaged area. As the load was increased to 267 N and 356 N (67% and 89% of N_{cr}), the number of cracks increased to 29 and 40, respectively. Out of all observed cracks, 86% were seen to grow larger than their size at initiation. At each load, nearly half of the observed cracks occurred in pairs, indicating some extent of interaction. Interestingly, nearly 85% of cracks were observed to initiate in regions of low fiber-volume fraction. These regions, which appear as dark gray in Fig. 9, were likely formed during tow spreading in the preimpregnation process. The remaining 15% of cracks initiated near the specimen's top edge, and these were likely influenced by presence microscopic machining flaws and/or surface irregularities. The ultimate failure of this, and all other specimens, was caused by rapid and unstable growth of a single dominant crack. In some cases, as evident from post-mortem surface analysis, the single dominant crack was triggered by interaction and coalescence of multiple smaller cracks. Finally, none of the observed macroscopic failure sites initiated from the observed surface microcracks, suggesting that final failure was always triggered on the specimens' interior.

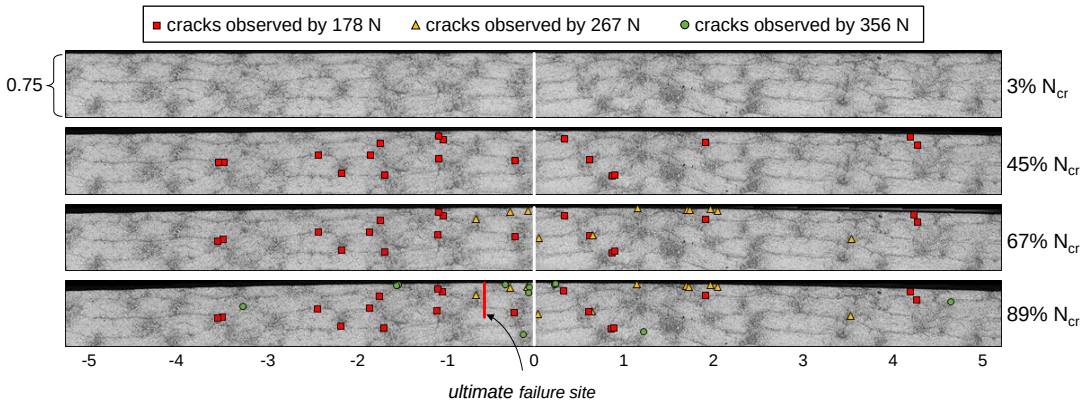

Figure 9. *In-situ* optical microscope observations of transverse microcracking during 3PB flexure testing (dimensions in mm)

The single and multi-image analysis described above was performed in similar detail for specimens that exhibited very low and high Y_T. These specimens, which represented the tail ends of Y_T distributions, were analyzed to determine whether the microstructure had any influence over the extreme values of Y_T. In general, no correlation was found between values of Y_T and any of the observable microstructural features. These features include frequency and location of microscale cracking, fiber clustering, presence of resin rich regions, and surface flaws. These observations suggest that extreme values of Y_T are controlled by combined effect of the microstructure, local mechanical fields, and local variability in the material properties (e.g. strength of the resin and resin-fiber interface).

The formation of internal microcracks, and depth of the surface microcracks, was investigated using the serial-sectioning method described in Sec. 2.2.1. An example of this investigation is presented in Figure 10, which shows subsequent sections of the same microstructural area imaged 0.2 mm below the top tensile edge, and 0.23 mm to the left of the center roller. The four shaded fibers in each image are used as fiducial markers indicating that the same area is being viewed.

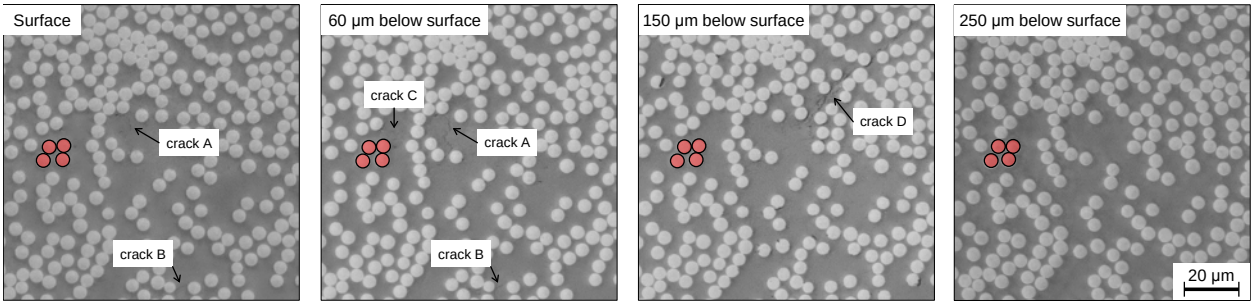

(a) (b) (c) (d)

Figure 10. Results of serial sectioning of the 3PB specimen

Examination of images in Fig. 10, and other similar regions, suggests that individual surface cracks do not propagate deep into the center of the specimen. In the example shown, the surface cracks (A and B) are visible 60 μm below the surface (Fig. 10b), but disappear in the next section

at 150 μm (Fig. 10c). Similarly, cracks C and D appear, respectively, at 60 and 150 μm below the surface (Fig. 10b-c), but disappear in subsequent sections shown in Fig. 10c-d. Examination of similar regions suggests that on average, at 80% of critical load, the microcracks were approximately 100 μm in length and 5-50 μm in width.

The microscale observations performed in this study, including those presented in Figs. 9 and 10, are used to hypothesize a sequence of likely microscale events that lead to macroscopic failure of the *flexure* specimens used to measure Y_T. This sequence, which is shown pictorially in Fig. 11, begins with formation of short transverse cracks that initiate at loads as low as 40% of N_{cr}. In general, these cracks appear to form in the region of high tensile stresses, which extends several millimeters away from the specimen's center in each direction. As the load is increased, additional cracks initiate within the highly stressed area and the existing cracks extend in length. Finally, when the load approaches N_{cr}, a single dominant crack, or a coalescence of multiple microcracks, becomes unstable, triggering macroscopic failure of the entire specimen. This sequence of events, *if correct*, may create a challenge in interpreting the meaning of Y_T. Given the clear evidence of microscale crack formation well before macroscopic failure, one can argue that Y_T represents a "structural" response of a given characterization specimen to accumulation and unstable growth of microscale damage. It remains to be seen whether this "apparent" material property can be used, with high confidence, to predict initiation of transverse failure in tape laminates. The microstructural observations presented in this study suggest that, at the very least, prediction of *microscale* transverse failure/fracture (i.e. at the scale of individual fibers) should be performed using a different material property measured at the microscale. The microscale fracture phenomenon, and in particular transverse microcrack coalescence, clearly requires further attention. Additional studies (e.g. utilizing X-ray computed tomography or

micromechanical modeling) are needed to fully understand the processes of microscale crack coalescence which may govern the statistical distribution of Y_T.

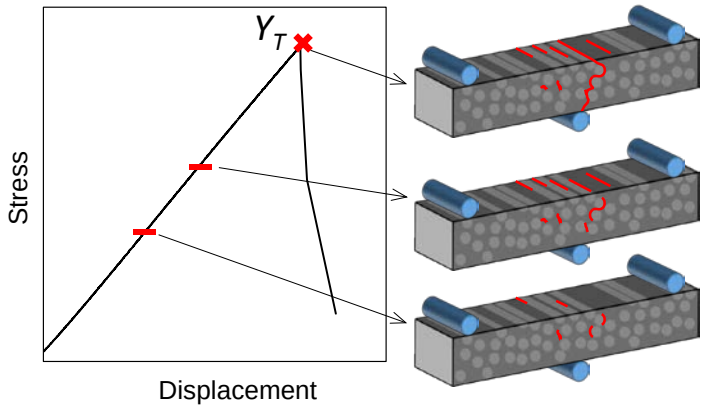

Figure 11. Proposed sequence of microscale events that leads to macroscopic failure of the 3PB flexure specimens

5. CONCLUSION

The aim of this study was to reexamine the way in which transverse tensile strength, Y_T, is characterized for tape-laminate polymer-matrix composites. To this end, Y_T was measured using 3-point bend (3PB), 4-point bend (4PB), and tensile specimens fabricated using IM7/8552 carbon/epoxy. Given the well-documented issues with existing transverse tensile tests, a new tensile dogbone specimen was developed to ensure consistent failure in the gage region. The three distinct specimen geometries were intentionally selected to investigate the relationship between specimens' effective volume (i.e. volume subjected to tensile stresses) and the magnitude and scatter of Y_T. In addition to Y_T characterization, a number of 3PB and 4PB specimens were polished on the transverse (2-3) planes, and monitored *in-situ* during strength testing. The *in-situ* observations were performed using a high-magnification optical traveling microscope capable of resolving cracks at the length scale of individual fibers. These observations, which were coupled with additional *ex situ* post-mortem imaging, were used to develop a possible explanation of why existing strength-scaling theories (vis. Weibull theory)

fail to properly model and scale the stochastic distribution of Y_T. Finally, additional 3PB specimens were used to examine the effect of specimen surface preparation (i.e. unpolished vs. polished), and specimen orientation (i.e. out-of-plane versus in-plane transverse failure) on Y_T.

The key findings resulting from this investigation include:

- The new tensile dogbone specimen configuration proposed in this study resulted in tensile failure that occurred consistently within the gage region. This specimen geometry provides a signification improvement over the current use of ASTM D3039 test method for characterization of Y_T in uniaxial tension.
- In all, a large number of specimens were tested using the 3PB, 4PB, and tensile test configurations, which offers a comprehensive survey of Y_T for IM7/8552. These tests confirmed that Y_T depends on the specimen volume and surface finish; however, Y_T seems to be insensitive to the direction of transverse failure. This latter observation is consistent with those made for other inter- versus intra-laminar mode I fracture toughness.
- The magnitude of Y_T was found to be inversely proportional to increasing effective volume, which is consistent with the Weibull statistical strength theory. Moreover, the 2-parameter Weibull theory was found to be an adequate model for scaling the characteristic value of Y_T among the three configurations considered. This notwithstanding, the 2-parameter Weibull theory provided a rather poor fit at the tails of Y_T distributions, which may result in overly conservative predictions of failure in numerical analysis.
- Detailed *in-situ* microscopic observations were performed on the tensile side of 3PB and 4PB specimens during testing. These observations revealed that nearly all specimens exhibited some amount of microcracking prior to catastrophic failure without measurable change in specimen compliance. Post mortem examination of tested specimens revealed microcrack

formation across the entire specimen width. These observations, and the proposed sequence of events leading to specimen failure, seem to violate the "weak-link" assumptions of the Weibull strength scaling theory.

- The currently accepted approach for using single deterministic values of Y_T in PDA analyses raises the question of which values (e.g. polished vs. unpolished, flexure vs. tension) should be used moving forward? As such, this question challenges the predictive capability of models where use of Y_T extends beyond prediction of damage onset (e.g. models that use traction-separation laws).

6. ACKNOWLEDGMENTS

The authors would like to thank Dr. T. Kevin O'Brien from NASA Langley, and Dr. Jacob Hochhalter from the Department of Mechanical Engineering at the University of Utah for their technical support. This work was supported by the NASA Advanced Composites Project [grant number NNX15AJ92A] with Dr. James Ratcliffe as the grant monitor.

REFERENCES

[1] S.T. Pinho, C.G. Dávila, P.P. Camanho, L. Iannucci, P. Robinson. 2005. "Failure Models and Criteria for FRP Under In-Plane or Three-Dimensional Stress States Including Shear Non-linearity." NASA/TM-2005-213530.

[2] C.A. Rose, C.G. Dávila, F.A. Leone. 2013. "Analysis methods for progressive damage of composite structures." NASA/TM-2013-218024.

[3] S.R., Hallett, M.R. Wisnom. 2006. "Numerical investigation of progressive damage and the effect of layup in notched tensile tests." *Journal of Composite Materials*, 40(14):1229-1245.

[4] C. Bouvet, B. Castanié, M. Bizeul, J.J. Barrau. 2009. "Low velocity impact modelling in laminate composite panels with discrete interface elements." *International Journal of Solids and Structures*, 46(14-15):2809-2821.

[5] N. Moës, J. Dolbow, T. Belytschko. 1999. "A finite element method for crack growth without remeshing." *Int. J. Numer. Methods Eng.* 46(1999):131-150.

[6] T. Belytschko, T. Black. 1999. “Elastic crack growth in finite elements with minimal remeshing.” *Int. J. Numer. Methods Eng.* 45(1999):601-620.

[7] F.P. Van der Meer, L.J. Sluys. 2009. “A phantom node formulation with mixed mode cohesive law for splitting in laminates.” *International Journal of Fracture*, 158(2):107.

[8] N. De Carvalho, B. Chen, S. Pinho, P. Baiz, J. Ratcliffe, T. Tay. 2013. “Floating Node Method and Virtual Crack Closure Technique for Modeling Matrix Cracking-Delamination Interaction.” NASA/CR-2013-218022.

[9] E.V. Iarve, M.R. Gurvich, D.H. Mollenhauer, C.A. Rose, C.G. Dávila. 2011. “Mesh-independent matrix cracking and delamination modeling in laminated composites.” *International Journal for Numerical Methods in Engineering*, 88(8):749-773.

[10] D.S. Dugdale. 1960. “Yielding of steel sheets containing slits.” *J. Mech. Phys. Solids.* 8 (1960):100-104.

[11] G.I. Barenblatt. 1962. “The Mathematical Theory of Equilibrium Cracks in Brittle Fracture.” *Adv. Appl. Mech.* 7(1962):55–129.

[12] A. Turon, P.P. Camanho, J. Costa, and J. Renart. 2010. "Accurate simulation of delamination growth under mixed-mode loading using cohesive elements: definition of interlaminar strengths and elastic stiffness." *Composite Structures* 92(8):1857-1864.

[13] A. Turon, P.P. Camanho, J. Costa, C.G. Davila. 2006. “A damage model for the simulation of delamination in advanced composites under variable-mode loading.” *Mech. Mater.* 38:1072–1089.

[14] K.H. Hoos, E.V. Iarve. 2018. "Discrete Damage Modeling of Matrix Dominated Failure Including Random Spatial Variation of Strength." In Proceedings of the American Society for Composites – 33rd Technical Conference on Composite Materials.

[15] ASTM Standard Test Method for Tensile Properties of Polymer Matrix Composite Materials, D3039/D3039M, 2008.

[16] T.K. O’Brien, S.A. Salpekar. 1993. “Scale effects on the transverse tensile strength of graphite/epoxy composites.” In Eleventh Volume: Composite Materials—Testing and Design. ASTM International.

[17] J.M.F. de Paiva, S. Mayer, M.C. Rezende. 2006. “Comparison of tensile strength of different carbon fabric reinforced epoxy composites.” *Mater. Res.* 9(1):83–90.

[18] I. De Baere, W. Van Paepegem, M. Quaresimin, J. Degrieck. 2011. “On the tension-tension fatigue behaviour of a carbon reinforced thermoplastic part I: Limitations of the ASTM D3039/D3479 standard.” *Polym. Test.* 30:625–632.

[19] T.K. O'Brien, A.D. Chawan, K. DeMarco, I. Paris. 2003. "Influence of specimen configuration and size on composite transverse tensile strength and scatter measured through flexure testing." *J Compos Tech Res*, 25(1):3-2.

[20] D.F. Adams, T.R. King, D.M. Blackketter. 1990. "Evaluation of the transverse flexure test method for composite materials." *Compos. Sci. Technol.* 39:341–353.

[21] R.E. Bullock. 1974. "Strength ratios of composite materials in flexure and in tension." *J. Compos. Mater*. 8:200–206.

[22] J.M. Whitney, M. Knight. 1980. "The relationship between tensile strength and flexure strength in fiber-reinforced composites." *Exp. Mech.* 20:211–216.

[23] M.S. Madhukar, L.T. Drzal. 1991. "Fiber-Matrix Adhesion and Its Effect on Composite Mechanical Properties: Tensile and Flexure Behavior of Graphite/Epoxy Composites." *J. Compos. Mater*. 25:958–991.

[24] M. Maalej, V.C. Li. 1994. "Flexural/Tensile-Strength Ratio in Engineered Cementitious Composites." *J. Mater. Civ. Eng.* 6:513–528.

[25] L. Biolzi, S. Cattaneo, G. Rosati. 2001. "Flexural/Tensile Strength Ratio in Rock-like Materials." *Rock Mech. Rock Eng.* 34:217–233.

[26] K.M. Prewo. 1986. "Tension and flexural strength of silicon carbide fibre-reinforced glass ceramics." *J. Mater. Sci.* 21:3590–3600.

[27] M.P. Hardy, J.A. Hudson, C. Fairhurst. 1973. "The failure of rock beams: Part I—Theoretical studies." *Int. J. Rock Mech. Min. Sci.*, 10:53-67.

[28] G. Swan. 1980. "Fracture stress scale effects for rocks in bending." *Int. J. Rock Mech. Min. Sci.* 17:317-324.

[29] Z.P. Bažant. 1984. "Size effect in blunt fracture: concrete, rock, metal." *J. Eng. Mech.* 110:518-535.

[30] G.D. Quinn, R. Morrell. 1991. "Design Data for Engineering Ceramics: A Review of the Flexure Test." *J. Am. Ceram. Soc.* 74:2037–2066.

[31] S. Nohut, A. Usbeck, H. Özcoban, D. Krause, G.A. Schneider. 2010. "Determination of the multiaxial failure criteria for alumina ceramics under tension–torsion test." *Journal of the European Ceramic Society*, 30(16):pp.3339-3349.

[32] Z. P. Bazant. 2000. "Size effect." *Int. J. Solids Struct.* 37:69-80.

[33] M.R. Wisnom. 1999. "Size effects in the testing of fibre-composite materials." *Compos. Sci. Technol.* 59:1937–1957

[34] W. Weibull. 1939. “A statistical theory of the strength of materials.” *Ingeniors Vetenskaps Akad.* 151:1–4.

[35] J.L. Le, Z.P. Bažant, M.Z. Bazant. 2011. “Unified nano-mechanics based probabilistic theory of quasibrittle and brittle structures: I. Strength, static crack growth, lifetime and scaling.” *J. Mech. Phys. Solids.* 59:1322–1337.

[36] L.S. Sutherland, R.A. Shenoi, S.M. Lewis. 1999. “Size and scale effects in composites: I. Literature review.” *Compos. Sci. Technol.* 59:209–220.

[37] M.R. Wisnom, M.I. Jones. 1996. “Size Effects in Interlaminar Tensile and Shear Strength of Unidirectional Glass Fibre/Epoxy.” *J. Reinf. Plast. Compos.* 15:2–15.

[38] M.R. Wisnom, B. Khan, S.R. Hallett. 2007. “Size effects in unnotched tensile strength of unidirectional and quasi-isotropic carbon/epoxy composites.” *Compos. Struct.* 84:21–28.

[39] J. H. Crews, R. A. Naik. 1993. “Measurement of multiaxial ply strength by an off-axis flexure test.” *In Eleventh Volume: Composite Materials—Testing and Design.* ASTM International.

[40] B.C. Salzbrenner, J.M. Rodelas, J.D. Madison, B.H. Jared, L.P. Swiler, Y. Shen, B.L. Boyce. 2017. “High-throughput stochastic tensile performance of additively manufactured stainless steel.” *J. Mater. Process. Technol.* 241:1–12.

[41] Y. Ng, J. Tomblin. 2011. “NCAMP Process Specification” NPS 81228, Revision B.

[42] J. Schindelin, et al. 2012. “Fiji: an open-source platform for biological-image analysis.” *Nature Methods* 9:676-682.

[43] Q. Tseng. 2015. “Template Matching and Slice Alignment – ImageJ Plugins”.

[44] M.R. Gurvich, A.T. DiBenedetto, S.V. Ranade. 1997. “A new Statistical distribution for characterizing the random strength of brittle materials." *J. Mater. Sci.* 32(10):2559–2564.

[45] “ASTM Standard Practice for Size Scaling of Tensile Strengths Using Weibull Statistics for Advanced Ceramics.” C1683, 2015.

[46] R. Jain. 2008. “Effective area and effective volume calculations for ceramic test specimens.” M.S. Thesis, Cleveland State University.

[47] F.W. Zok. 2016. “On weakest link theory and Weibull statistics.” *J. Am. Ceram. Soc.* 1265-1268.

[48] F.N. Nwobi, C. Anderson Ugomma. 2014. “A Comparison of Methods for the Estimation of Weibull Distribution Parameters.” *Metod. Zv.* 11:65–78.

[49] G.E. Andrews, R. Askey, R. Roy. 2000. “Special functions.” *Cambridge University Press*, Vol. 71.

[50] T.K. O’Brien, R. Krueger. 2001. “Analysis of Ninety Degree Flexure Tests for Characterization of Composite Transverse Tensile Strength.” NASA/TM-2001-211227.

[51] MATLAB Release 2014a, The MathWorks, Inc., Natick, Massachusetts, United States.

[52] “Hexcel 8552 IM7 Unidirectional Prepreg 190 gsm & 35%RC Qualification Material Property Data Report,” NCAMP Test Report Number: CAM-RP-2009-015 Rev A, April 22, 2011.

[53] B.L. Boyce. 2010. “A Sequential Tensile Method for Rapid Characterization of Extreme-value Behavior in Microfabricated Materials.” *Exp. Mech.* 50:993–997.

[54] M.W. Czabaj, J,G. Ratcliffe. 2014. "Comparison of intralaminar and interlaminar mode I fracture toughnesses of a unidirectional IM7/8552 carbon/epoxy composite." *Composites Science and Technology* 89: 15-23.